Frequency Regulation of a Standalone Interconnected AC Microgrid Using Innovative Multistage TDF(1+FOPI) Controller

H. Shayeghi *,A. Rahnama*

Energy Management Research Center, University of Mohaghegh Ardabili, Ardabil, Iran

Abstract *- This paper's main purpose is to offer an innovative multistage controller for load-frequency regulation of a standalone interconnected microgrid (SMG). A multistage TDF(FOPI+1) controller is designed, with the first stage being a filter built of the tilting and derivative operators. Transferring the integrator component to the second stage of the controller and employing its fractional-order (FO) form as a FO proportional-integrator (FOPI) controller results in the latter stage of the controller. To calculate the optimal controller parameters, the recently introduced Bonobo optimization algorithm (BOA) is applied. Besides, the optimization objective function is a mix of the control error signal in each area and the dynamic response characteristics of the system. In complex operating conditions such as sudden changes in power demands, uncertainties in renewable energy units' output, considering nonlinear factors, and parametric uncertainties in a two-area SMG, the performance of the proposed controller is compared with classical and multistage controllers. The results show that the TDF(1+FOPI) controller has a competent dynamic response and can be a suitable choice for performing LFC duties in SMGs. This control strategy's advantages include enhanced controller resistivity in diverse circumstances, faster reaction times, and better dynamic behavior. The results of the five studied scenarios show that using the proposed control strategy, the value of the objective function is improved by an average of more than 50% compared to other classical and conventional controllers. Similarly, improvements of more than 70% and 50% in key integral of time-weighted square error (ITSE) and Integral of absolute error (IAE) time zone indicators, respectively, are among the results of these studies.*

Keyword—Bonobo optimization algorithm, Load-frequency control, Standalone microgrids, TDF(1+FOPI) multistage controller.

NOMENCLATURE

α	Order of the integrator controlling action
Δf	Frequency deviations
P_{tie}	Tie-Line power
P_{DG}	Output power of the DG unit
$P_{L,j}$	j^{th} area's load
T_{sim}	Simulation time
D	Damping coefficient
f	Frequency
j	Area index
M	Inertia constant
N	Derivative filter coefficient
WT	Wind turbine
K_D	Derivative control operator gain
K_I	Integral control operator gain
K_P	Proportionalcontrol operator gain
K_T	Tilted control operator gain
ΔP_{tie}	Tie-line power deviations
N_b	The number of bonobos
P_{BES}	Output power of the BES unit
P_{PV}	Output power of the PV unit
P_{SMES}	Output power of the SMES unit
P_{WT}	Output power of the WT unit
It	Iteration

ACE	Area control error
BES	Battery energy storage
BOA	Bonobo optimization algorithm
DG	Diesel generator
ESS	Energy storage system
FO	Fractional order
IAE	Integral of absolute error
ISE	Integral of square error
ITAE	Integral of time-weighted absolute error
ITSE	Integral of time-weighted square error
LFC	Load frequency control
MG	Microgrid
MOS	Maximum overshoot
MUS	Maximum undershoot
OF	Objective function
OS	Overshoot
PV	Photovoltaic panel
RES	Renewable energy sources
SMES	superconducting magnetic energy storage
SMG	Standalone microgrid
ST	Settling time
US	Undershoot

1. INTRODUCTION

MGs now play a critical role in supplying the power needs of various users. MGs are small-scale power systems that contain a variety of distributed power sources, ESSs, consumers, and control mechanisms. Using a greater range of RESs is one of the key advantages of MGs [1]. Despite the fact that RESs are ecologically favorable and inexpensive, the extensive integration of RESs into the power supply system's structure brings obstacles. Power electronic interfaces connect RES-based power generation units to the power system. As a result, MGs have less inertia than traditional power systems, making it challenging to keep the system frequency within

the acceptable range [2]. The malformed system frequency can cause serious damage to network components and frequency-sensitive loads. So, it is critical to establish system stability in MGs with fewer ancillary services [3]. Moreover, RESs have a poor ability to provide backup power to support system frequency stability, so SMGs necessarily must have backup units. SMGs are an opportunity to realize the concept of "local generation, local consumption." DGs are a common option for backup power. ESSs such as batteries, flywheels, and SMESs are widely used in MGs to ensure power generating quality and reliability. Methods for resolving imbalances in power systems include those with ESS and those without ESS. Studies show that the presence of ESS in the system makes it possible to repel system frequency fluctuations in a desirable way. Because compared to systems without storage, they have the ability to support the system with additional power [5]. However, system frequency stability cannot be achieved without proper controllers. Implementing robust control techniques to address power generation and consumption mismatches in SMGs is much more critical where there is no main network assistance [3, 5]. Various control strategies have been used to perform the load-frequency control task in MGs. Their primary joint responsibility is balancing power production and consumption and regulating power flow between areas in interconnected structures to keep the system stable [6]. The traditional controllers such as proportional integrator (PI) and proportional integral derivative (PID) do not perform satisfactorily in complex working conditions, especially in the face of nonlinear factors, despite their simple structure and proper operation [7]. By supplanting the proportional part of the PID controller with a tilted component, TID controllers are introduced. The studies show that by using the tilted operator with $S^{(}-1/n)$ transfer function, the TID controller performed better than I, PI, and PID controller in establishing the frequency stability of MGs [8]. The limitations of derivative and integral control operators are a challenge that can be overcome by using FO operators in the design of controllers [9, 10]. By increasing the degree of freedom of the controllers, FO operators enable better dynamic behavior. The FO control operators have been used to control of many systems and their practical functions have been studied [11]. Hardware implementation of FO controllers in industrial systems has also been reported [12]. In the power systems field, the FO form of the conventional PID (FOPID) controller is also applied to establish frequency stability in with electric vehicles integration [13]. However, achieving optimal performance on controllers with parallel structures is not easy. Because the operation of the control actions directly affects each other and, consequently, the control output signal, making it challenging to reach a suitable trade-off among the components [14]. One way to get rid of this predicament is to change the configuration of the controllers. Controllers with multistage structures can be eliminated the shortcomings of parallel structures significantly. Various multistage controllers are used in the LFC of SMGs [14–16]. Using FO operators in multi-level controllers is an approach that aims to take advantage of both FO control operators and multistage configuration together [17]. It should be emphasized that LFC problems are complex, and FO operators add optimization parameters, increasing the problem's dimensions. It makes solving optimization problems more challenging. Thus, increasing the control handles is not always beneficial and may result in a deviation from the ideal control design.

In addition to the controllers mentioned earlier, other controllers have been employed to control the frequency of various power systems. Fuzzy logic-based controllers, adapted to diverse operating conditions, have been frequently used to solve the LFC problems [18, 19]. Despite their versatility, these controllers' reliance on expert knowledge and the effects of membership functions on their performance is cumbersome [20]. The use of sliding mode controllers in regulating the frequency of SMGs, including electric vehicles, has been reported in [5]. The coordinated use of droop and sliding mode controllers in the first and second control layers has also been studied [21]. Model predictive controllers (MPC) have been studied to improve SMGs' voltage and frequency control, including ESSs [4]. Complexities of the design and coordination required to govern various power generation sources, using the MPC technique to control complex multi-area SMGs is cumbersome. Abubakr et al. used the online tuning approach of controllers to preserve the stability of SMGs by providing virtual inertia support [22]. This strategy's reliance on the speed and precision of the method for figuring out the optimal controller settings and the effects of delay on the control system's performance is debatable. Ali et al. have developed a coefficient diagram method (CDM)-based virtual inertia control approach to address the issue of low inertia in SMGs [23]. In this strategy, uncertainty in system parameters is a significant issue since this strategy for high performance is heavily dependent on the validity of system component models. In a power system, improper controller functions can result in energy loss, reduced power quality, undesirable dynamic behavior in changing system operating points, damage to network equipment and devices, system instability, or even blackouts [24]. Therefore, optimal adjustment of the controller parameters is essential. The LFC problem-solving technique is a cornerstone of any success in achieving well-adjusted controllers. To accomplish the desired system behavior, diverse strategies have been employed to identify the appropriate controller variables[3]. Today, because of significant and increasing breakthroughs in the soft computing field, employing meta-heuristic optimization algorithms in the design of controllers is a common strategy with appropriate response accuracy [14]. Population-based nature-inspired algorithms are among the most prominent strategies for tackling controller optimization problems to execute the LFC task [25]. The gray wolf optimization (GWO) algorithm is used to optimally adjust the fuzzy PID controller parameters in order to establish the frequency stability of a hybrid power system [26]. The optimal PID controller settings in an interconnected power system, taking into account RESs, different uncertainties, and nonlinearities, have also been determined using the marine predator algorithm [27]. The proper formulation of the OF is an important requirement for reaching the optimal controller setting in addressing the LFC problem. OF is the mathematical expression of the controller's behavior as expected by the designer. Various OFs have been used as OF to design controllers such as IAE, ISE, and their time-weighted forms (i.e., ITAE and ITSE) [3, 28, 29].

Motivated by what is mentioned, this study introduces a new controller, TDF (FOPI+1), introduced in a multistage design using FO operators. The proposed structure in the first stage consists of tilted and derivative operators that act as filters, and this stage's output is the second stage's input. A FOPI controller is used in the second stage. Previous studies have demonstrated that separating parallel structures and transferring the integrative control operator to subsequent layers enhances response speed. Here, while transferring the integration action to the second stage, its FO form is used. According to the findings of the investigations, the proposed configuration, although providing improved dynamic characteristics than controllers such as PID and TID utilizing titled and FO operators, gives better responses than PD(1+PI) controllers with classical form. The BOA is used to optimize the controller parameters [30]. ITAE is defined as OF in combination with the MOS and MUS dynamic response characteristics values for proper controller operation. Following the design, the suggested controller is tested without retuning under a variety of scenarios such as abrupt changes in demand, uncertainties in RESs generation, nonlinear factors, and uncertainties in system characteristics. Also, the performance of the proposed controller is compared with the classic PID controller introduced in the [19], whose parameters are optimized by the grasshopper optimization algorithm (GOA). The TDF(1+FOPI) controller is clearly better than other traditional and powerful controllers, according to evaluations. The salient contributions of this work are digested as below:

(i) As a new controller, a multistage TDF(1+FOPI) has been introduced to govern system frequency irregularities and preserve system stability.

(ii) The recently announced BOA identifies the controller parameters by minimizing an atypical OF, including ITAE, MOS, and MUS of the system's dynamic response to achieve robust performance.

(iii) (iii) The dynamic behavior of the system under various operating conditions is analyzed, including variations in power demand and RES output, the effect of time delay as a nonlinear factor, and uncertainty in system parameters.

(iv) (iv) The TDF(1+FOPI) results are contrasted with the results achieved by applying the PID, TID, and PD(1+PI) controllers optimized with BOA to emphasize better and demonstrate the proposed performance controller.

Whatever is included in the remainder of this article is sorted out as follows. The understudy SMG modeling is portrayed in Section 2. Section 3 elucidates the synthesis of the TDF(1+FOPI) multistage controller. Section 4 presents the OF formulation and discusses problem-solving using the BOA to reach the optimal controller. Section 5 shows the outcomes of the control strategy evaluations in various scenarios and comparisons. At long last, in Section 6, the conclusions are stated.

2. STUDY CASE

2.1. Dynamic Model

The use of frequency-domain dynamic models is common for LFC studies in MGs. The order of an MG's dynamic models is generally high [31]. Numerous investigations have revealed that, while having exceptional accuracy, the usage of lower-order linear models is well-matched with the outcomes of hardware tests [5, 32]. This paper has extracted the simplified dynamic models of various units using references [10] and [19]. Figure 1 shows the dynamic representation of the two-area SMG system, and the relevant parameters are presented in Table 1 [19]. As power generation sources, the system incorporates DG, PV arrays, WTs, ESSs including BES system and SMESs, and AC 'loads in both areas. Because of their limited reserve capacity and uncertain nature, RESs generally do not participate in LFC undertakings.

2.2. Power Generation Units of the SMG

1) Diesel Generator

In order to satisfy the generation-consumption balancing situation dependent on the output of RESs and load demand, standby DGs operate autonomously. The torque produced by the diesel engine drives the synchronous machine, which generates the electrical output. Due to consumers' abrupt changes in power demands, it is crucial that the diesel prime mover have a quick dynamic response and strong disturbance rejection capabilities. Equation (1) mimics the dynamic model of the actions between DG's inlet valve and engine [14].

$$G_{DG}(s) = \left(\frac{K_g}{1 + T_g s}\right)\left(\frac{K_t}{1 + T_t s}\right) \quad (1)$$

2) Wind Turbine

A WT's output power depends on the wind speed. It is impossible to create electricity for WT if the wind speed is below a specific limit (V_{cut-in}), and it is also harmful for WT if the wind speed is higher than the permissible limit ($V_{cut-out}$), therefore the producing power will be zero. In [33], the horizontal axis WT's behavior is effectively represented. A first-order transfer function as (2) can be used to represent WT dynamic response model [15, 31].

$$\frac{\Delta P_{WT}}{\Delta P_w} = \frac{K_{wt}}{1 + s T_{wt}} \quad (2)$$

Table. 1: Understudy SMG dynamical model parameter values

Parameter	Value	Parameter	Value
K_{pv}, T_{pv}	1, 1.5 s	K_{BES1}, K_{BES2}	-10, -8
K_{wt}, T_{wt}	1, 1.5 s	T_{BES}	0.1 s
K_g, T_g	1, 0.1 s	T_{SMES}	0.03 s
K_t, T_t	1, 0.4 s	$T_1, T_2,$	0.233 s, 0.7087 s,
$M_1, D_1,$	0.8, 0.02	T_3, T_4	0.016 s, 0.2481 s
M_2, D_2	0.7, 0.03	K_{SMES1}, K_{SMES2}	-0.2461, -0.2035
B_1, B_2	10, 12.5	T_{12}	3.2π
R_1, R_2	0.05, 0.04	α_{12}	-1

3) Photovoltaic

The intensity of sunlight and the surface temperature determine the electrical energy that can be extracted from PVs at any given time [18, 33]. For frequency domain studies, the following first-order transfer function provides an acceptable model of PVs:

$$\frac{\Delta P_{pv}}{\Delta \phi} = \frac{K_{pv}}{1 + s T_{pv}} \quad (3)$$

4) BES System

Recently, it has been demonstrated that BES System can quickly manage its active and reactive power output at switching frequencies much over the kHz range. While load balancing, harmonic cancellation, and voltage control are typically its primary uses, once placed, the BES equipment also can be used to add extra damping to power system oscillations to enhance both transient and dynamic stability. A simple first-order transfer function expresses the dynamic model of the BES system as follows [34]:

$$\frac{\Delta P_{BES}}{\Delta f_j} = \frac{K_{BES}}{1 + s T_{BES}} \quad (4)$$

5) SMES

The transfer function of the SMES G_{SEMS} (s), which has a quick frequency response, complies with (5). In this case, the SMES excitation signal is Δf, while in studies of the conventional power systems, the ACE_j signal has also been utilized [10, 35].

$$\frac{\Delta P_{SMES,j}}{\Delta f_j} = K_{SMES,j}\frac{(1 + T_1 s)(1 + T_2 s)}{(1 + T_3 s)(1 + T_4 s)}\left(\frac{1}{1 + T_{SMES} s}\right) \quad (5)$$

3. CONTROLLER DESIGN

The suggested TDF(1+FOPI) controller's basic idea is to combine correct and fractional control operators in a multistage configuration. This section discusses the suggested controller structure after a brief synopsis of FO calculations.

3.1. FO Calculation

Integration and derivation in noninteger orders fall into the realm of fractional calculations. Simply, $_aD_t^r$ is a generalized continuous integral-differential operator, abbreviated as (6) [36]:

$$_aD_t^r = \begin{cases} d^r/dt^r & \Re(r) > 0 \\ 1 & \Re(r) = 0 \\ \int_a^t (d\tau)^{-r} & \Re(r) < 0 \end{cases} \quad (6)$$

where a and t represent the operator range, and $r \in R$ is a real number indicating the order of the operator. In recent years, the application of FO operations in different engineering disciplines, such as system modeling and automatic control, has been addressed [9]. The four basic types of FO utilization in the control field are FOPID, CRONE control, fractional type lead-lag compensators, and TID controller [37]. Combining control operators in various configurations is drawn from these primary types.
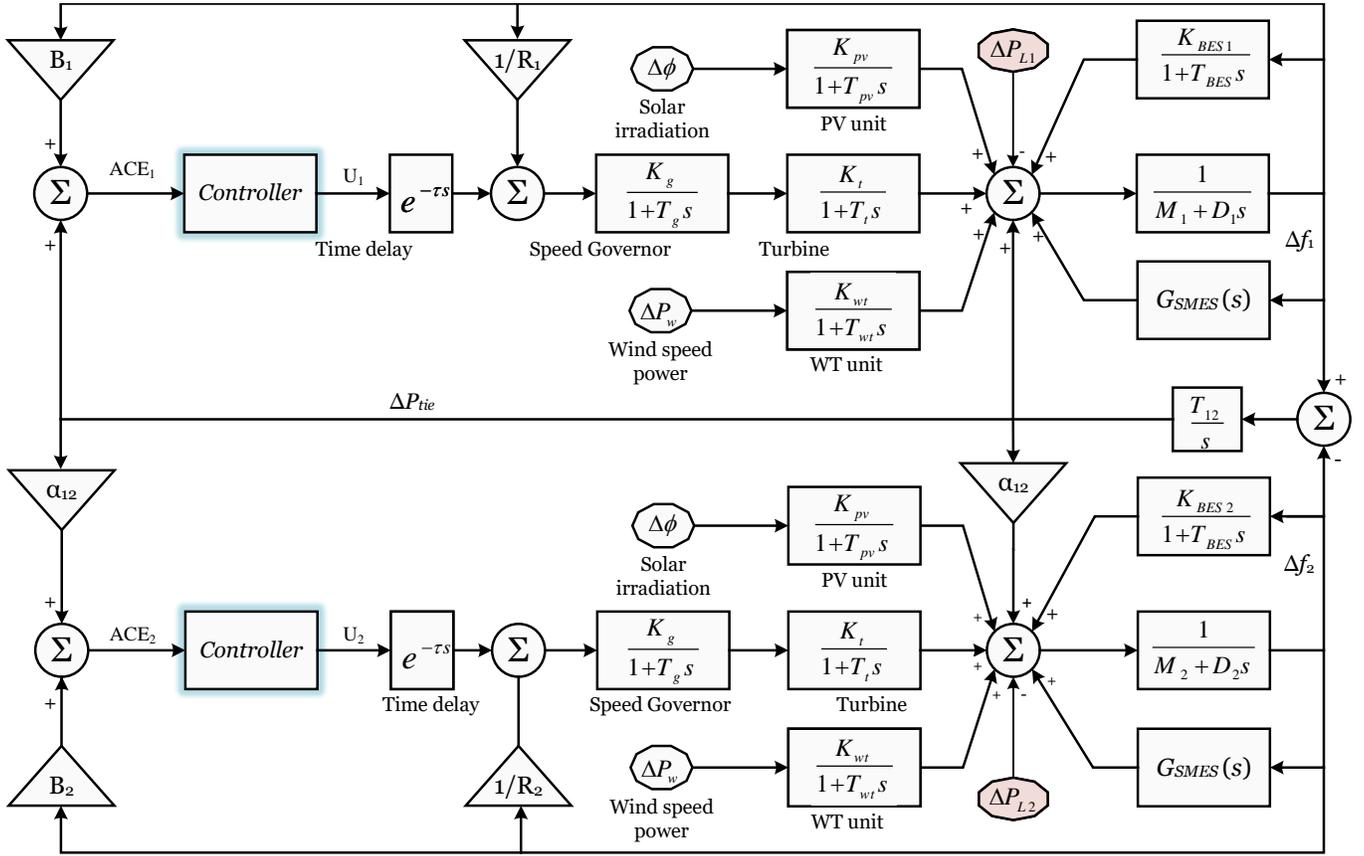
Fig. 1: Frequency response model of the understudy interconnected SMG

The primary idea behind employing multistage controllers is to reduce the unavoidable impacts of control operators on one other in parallel processing. To obtain optimal control performance in parallel structures, a compromise between distinct actions is required. Recourse to compromise implies that the operators' full ability is not utilized. As a result, while obtaining high performance in parallel arrangements is possible, a portion of the control operators' capability has been overlooked. Thanks to multi-layer designs, the control components can employ their maximum potential at each controller stage.

3.2. Proposed TDF(1+FOPI) Controller

The primary concept behind the proposed controller is to mix integer and noninteger-order operators in a multistage architecture. The tilting operator provides feedback gain as a function of frequency using the $S^{-1/n}$ transfer function. TDF is the proposed controller's primary phase that serves as a filter and is formed by mixing the tilted component with the derivative operator. The LFC process's control signal may be contaminated with noise. The TDF controller's initial part performs as a filter and can suppress high-frequency noises.

The inclusion of integrator operators into the controller design is required to abolish steady-state errors. However, raising the gain of this operator in the controllers with parallel structures degrades the control system's performance, particularly during the transient period. Moreover, every control activity may have unintended repercussions in addition to its efficient control impacts. Generating infinite gain at zero frequency and causing phase lag is one of the integrator operator's probable difficulties. This may be remedied with the aid of FO operators [36]. In addition, bringing FO calculations to controller design provides a broader leeway for designers. The preceding level's control signal is used as input in the second level

of the proposed controller, and the summation of this signal and what is generated after processing in a FOPI controller provides the controller's overall output. So, the second stage of the controller has the form (1+FOPI).

At last, the mathematical representation of what has been stated is given below:

$$U_c = G_{FOPI}\left(s, \theta\right) U_1\left(s\right)$$
$$U_1 = G_{TDF}\left(s, \gamma\right) ACE(s) \tag{7}$$

where ACE for j^{th} area can be calculated as below:

$$ACE_j(s) = B_j \Delta f_j(s) + \Delta P_{tie,j}(s) \tag{8}$$

In (7), $\theta \in R^3$ and $\gamma \in R^3$ are the proposed controller's first and second stage's controlling parameters where $\theta^T = \begin{bmatrix} K_T & n & K_D & N \end{bmatrix}$ and $\gamma^T = \begin{bmatrix} K_P & K_I & \alpha \end{bmatrix}$. For tilted operator, n is real and non-zero, ideally laid in a range between 1 and 10. The transfer function of the $G_{FOPI}(s, \theta)$ and $G_{TDF}(s, \gamma)$ are expressed in (9) and (10), respectively.

$$G_{TDF}(s, \theta) = \frac{K_T}{s^{1/n}} + K_D \left(\frac{N}{N + s}\right) s \tag{9}$$

$$G_{FOPI}(s, \gamma) = K_P + \frac{K_I}{s^\alpha} \tag{10}$$

Finally, TDF(1+FOPI) is the suggested controller's final configuration, as represented in Fig. 2.

To minimize the steady-state error in the LFC task, the integrator component gains must be raised, resulting in a loss of functionality of the controllers with a parallel configuration like PID or TID controllers in transient mode. Generally, it is preferable to have an idle or standby the integrator part of the controller in transient mode.
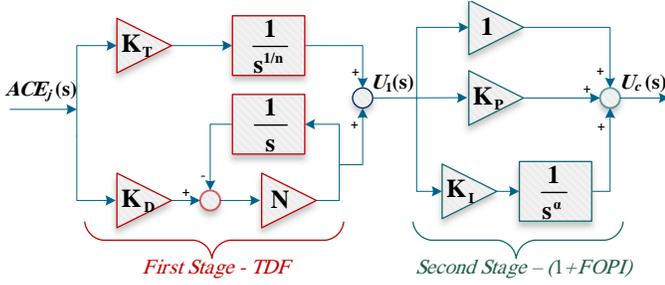
Fig. 2: Proposed TDF(1+FOPI) controller

So, to address this problem and effectively manage load frequency irregularities in an interconnected SMG, the TDF(1+FOPI) controller is presented, where the integrator is employed in the controller's second part. Besides, the proposed configuration's first layer uses a first-order derivative-based filter that ensures the suppression of high-frequency disturbances that various noise sources might produce during automated control.

4. OPTIMIZATION PROCESS

The controller's proper response is contingent on its suitable adjustment based on design priorities. The OF and technique of solving the optimization problem are pivotal for this purpose. Several criteria manifest the system's dynamic features based on error signals, such as frequency and tie power deviations (Δf and ΔP_{tie}). This section goes into finding the best fit with the aid of BOA after identifying the optimization criteria for tackling the LFC problem.

4.1. Objective Function

The ITAE index, while encapsulating the sum of the error signals, multiplies the time corresponding to the magnitude of the error at each timeframe, stressing the necessity for steady-state error resolution. As a result, the LFC mechanism allows a fluctuating dynamic response in the initial moments. Excessive frequency violation of the set points, on the other hand, may result in costly system degradation. As a result, OF is defined as (11) to strike an appropriate balance between transient behavior and control system dynamic response.

$$OF = ITAE + \lambda \left(MOS_{\Delta f_j} + MUS_{\Delta f_j} \right) \quad (11)$$

where, the ITAE index is formulated as (12), and $MOS_{\Delta f_j}$ and $MUS_{\Delta f_j}$ are expressed in (13).

$$ITAE = \sum_j \left(\int_0^{t_{sim}} t \left| \Delta f_j \right| dt \right) + \omega \int_0^{t_{sim}} t \left| \Delta P_{tie} \right| dt \quad (12)$$

$$\left\{ \begin{array}{l} MOS_{\Delta f_j} = \max \left(0, \Delta f_j \right) \\ MUS_{\Delta f_j} = \left| \min \left(0, \Delta f_j \right) \right| \end{array} \right. \quad (13)$$

In (11), λ is a weighting factor that regulates the exigence of MOS and MUS in the resulting dynamic response. Similarly, ω determines the effect of tie-line power fluctuations on the OF magnitude. The controller designer determines these weights depending on the desired purpose and functionality.

4.2. Optimization Method

Bonobos, like humans, belong to the Homininate subfamily. They live in communities, and each community breaks into smaller groups of differing sizes (fission), which re-merge on a regular basis (fusion) for various activities. The BOA is inspired by the reproductive activities of bonobos. The benefit of this search mechanism is

that its parameters are self-adjust. When using BOA to solve optimization problems, it is only required to specify the number of bonobos and the termination condition. According to the findings of the investigations, BOA has a strong performance, particularly in exploitation. In this algorithm, the community leader (i.e., alpha Bonobo) demonstrates the best ultimate solution to the optimization problem. The condition of society with the probability of p_p is separated into positive and negative phases (PP and NP) in this procedure. PP denotes a stable condition with food resources, living security, and so forth, whereas NP denotes an unstable environment. Four behaviors occur in the mating process of population members depending on whether the PP or NP condition is realized:

- Promiscuous: both the alpha and other lower-ranking male members take part;
- Restrictive: dominant males limit others;
- Consortship: a couple tends to leave the community as a partner and returns after a few days;
- Extra-group mating: females consider leaving the group and become engaged with males from other neighboring societies

Promiscuous and restricted actions occur in the PP condition, whereas the other two behaviors occur in the NP state. Figure 3 depicts the problem-solving procedure employing the BOA as a flowchart. More detailed information on community splitting, offspring generation process, and alpha bonobo updates are available in [30].

5. RESULTS AND EVALUATIONS

The BOA-based optimized TDF(1+FOPI) controller is assessed in this part. The investigation is carried out in six distinct circumstances. To highlight the proposed controller's quality, comparisons are conducted with the PID, TID, and PD(1+PI) controllers, which transfer functions are described as (14)– (16).

$$G_{PID}(s) = K_P + \frac{K_I}{s} + K_D \left(\frac{N}{N+s} \right) s \quad (14)$$

$$G_{TID}(s) = K_T \frac{1}{s^{1/n}} + \frac{K_I}{s} + K_D \left(\frac{N}{N+s} \right) s \quad (15)$$

$$G_{PD(1+PI)}(s) = \left(K_P + K_D (\frac{N}{N+s})s \right) \left(1 + K_{PP} + \frac{K_I}{s} \right) \quad (16)$$

It is helpful to provide numerical indications in addition to system frequency response graphs for better comparisons. To that end, the values of the ITSE and IAE indices, whose formulae are presented in (17) and (18), are reported alongside the values of the OF in each scenario.

$$ITSE = \sum_j \left(\int_0^{t_{sim}} t \Delta f_j^2 \, dt \right) + \omega \int_0^{t_{sim}} t \Delta P_{tie}^2 dt \quad (17)$$

$$IAE = \sum_j \left(\int_0^{t_{sim}} \left| \Delta f_j \right| dt \right) + \omega \int_0^{t_{sim}} \left| \Delta P_{tie} \right| dt \quad (18)$$

The MATLAB/Simulink environment is used to implement the SMG model. To model the FO operators, it is usual to use higher-order integer approximations with a negative real part and a limited frequency range as $[\omega_b, \omega_h]$, known as the Oustaloup method [36, 38]. The FOMCON toolbox for implementation of the FO controllers with $\omega_b = 10^{-3} Hz$ and $\omega_h = 10^3 Hz$ has been employed [39]. The value of the ω and λ in the OF are experimentally set to 0.8 and 2, respectively. The starting number of bonobos is set to $N_b = 30$, and the stop condition is set at 100 iterations ($It = 100$). Step load changes as +0.5 in area 1 and +0.7 in area 2 are applied for tuning the controllers' parameters, where the simulation time is set to 50 s. Also, an overview of solving the LFC problem and determining the optimal controller
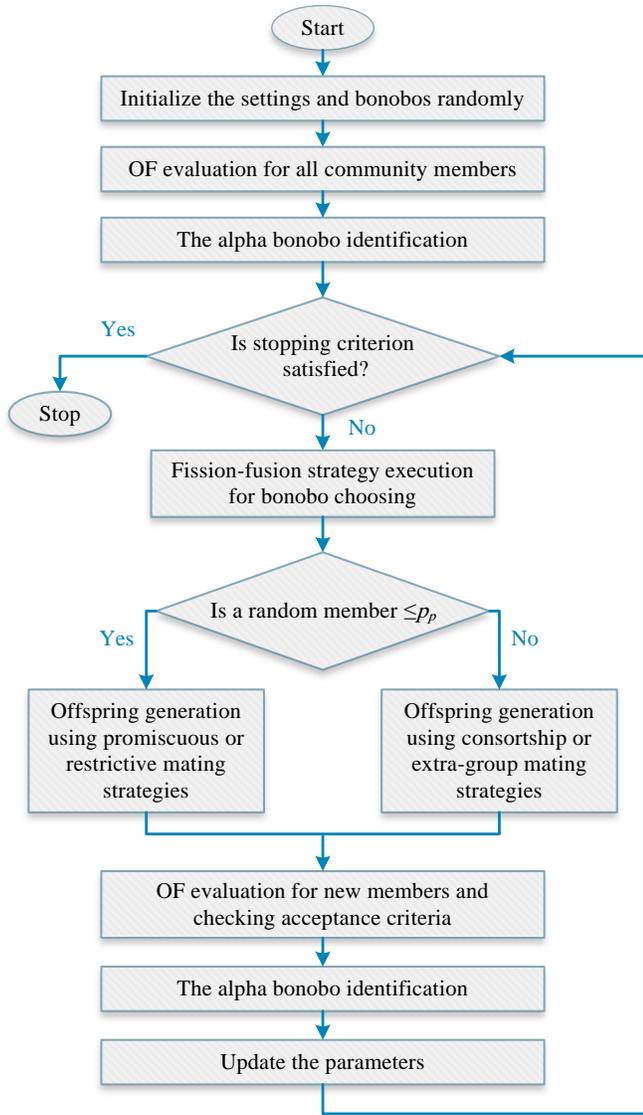
Fig. 3: Flowchart of the problem-solving process with BOA

parameters is given in Fig. 4. Table 2 show the optimal values of the controller parameters after optimization. The BOA convergence graph for controllers' parameters optimization is shown in Fig. 5. In the following, the controllers' performance is tested in six distinct conditions without recalibrating their settings.

(i) Load changes

The load fluctuations (ΔP_L) according to Fig 6 is examined in this case. The oscillations in frequency and power are illustrated in Fig. 7. Table 3 also includes the values of the performance evaluation indicators for accurate analysis. The examination of this situation reveals that the system's

behavior with the help of the TID and PD(1+PI) controllers is favorable than the PID controller. The results reveal that the TDF(1+FOPI) innovative control strategy outperforms the other controllers in terms of ITSE, IAE, and OF indicators, and also have better responsiveness, and MOS and MUS characteristics. In this scenario, the suggested controller improves the value of the OF, by an average of 56% when compared to the other three controllers. Similarly, the ITSE and IAE indicators have slumped by an average of 69 and 55%, respectively. At $t = 10s$, with increasing demand in area 1 and simultaneously decreasing demand in area 2, the tie power control becomes more complex. In this situation,

it is observed that the maximum tie power deviation value using TDF(1+FOPI) controller does not exceed 0.0453 p.u, while with the PID, TID and PD(1+PI) controllers, this value reaches 0.0645, 0.0660 and 0.0595 p.u, respectively.

(ii) RESs output power uncertainties

The nature of RESs such as WT and PV units is tainted with uncertainty. The benefit of the RESs positive features is possible only when appropriately confronted with their output oscillations. The output powers of the RES are considered in this situation, as illustrated in Fig. 8. In such instances, the system's dynamic behavior is depicted in Fig. 9. Table 3 also includes comparative indicators.

Using the proposed control technique, the OF values, as well as the ITSE and IAE indices, is diminished by an average of 55, 77, and 52%, respectively. Additionally, as shown in Fig. 9, the effect of changing the output power of RES from one region to another is reduced with the intervention of the suggested controller. This shows that the proposed controller has a faster acting speed in establishing the production-consumption balance in one area, preventing the error elimination time from being prolonged and the appearance of negative impacts in surrounding areas. Also, the maximum frequency deviation ($max\,(|\Delta f_j|)$) has been improved with the help of the TDF(1+FOPI) controller. In area 1, $max\,(|\Delta f_1|)$ values decreased by 35, 52, and 48% compared to the situation where the PID, TID, and PD(1+PI) controllers are employed. While in area 2, $max\,(|\Delta f_2|)$ is decreased by more than 50% averagely.

(iii) Parametric uncertainties

The most precise mathematical models of systems are also approximate representations of their actual dynamic behavior. If the control system is unsatisfactory, uncertainties in system parameters have undesirable implications. In this scenario, the parameters of the load and inertia model (D, M) are considered uncertain, so the value of M in both areas increases by 40%, and in contrast, the value of D decreases by 40%. Applied disturbances in the RESs output and electricity consumption are depicted in Fig. 10 over a 20-second timespan. Figure 11 depicts the dynamic reaction of the system, whereas the values of the evaluation indicators for comparison are given in Table 3.

Table 3 demonstrates the suggested controller's clear advantage in terms of assessment metrics. Despite the fact that all four controllers meet the system's stability requirements in this situation, the value of the OF with the TDF(1+FOPI) controller is about 56% lower. Also, the values of ITSE and IAE indices have improved on average by 74 and 54%, with the help of the proposed controller. Compared to the PID, TID, and PD(1+PI) controllers, the $max\,(|\Delta f_j|)$ value has improved by an average of more than 30% in both control areas.

(iv) Time-delay effect

Delay in receiving/sending control signals is one of the causes of nonlinear behavior in system responses. In this scenario, a delay of half a cycle at a frequency of 50 Hz ($\tau = 10\ ms$) is considered in sending the control signal. Perturbations in the form of +0.8 and +0.7 steps are applied in area 1 and area 2, respectively, while other system characteristics remain intact from the controllers' initial design circumstances. Here, in addition to the time-domain indicators' values listed in Table 3, the dynamic response characteristics of the system (Fig. 12), including OS, US, and ST for area frequency deviations and tie power fluctuations, are reported in Table 4. According to Table 3, most violations from the system's nominal frequency in areas 1 and 2 have decreased by an average of 48 and 56 %, respectively. Besides, the proposed controller improves the OF value by an average of 66 percent as compared to the use of the other three controllers. Under these conditions, the OF's value has been lowered by more than 80% compared to the typical PID controller. Compared to the other three controllers, this reduction is around 60%, on average. According to Table 4, the US index of Δf_1, Δf_2, and ΔP_{tie} signals is predominantly better when the controller TDF(1+FOPI) is used. Also, the average value of ST index has been improved by 6% for
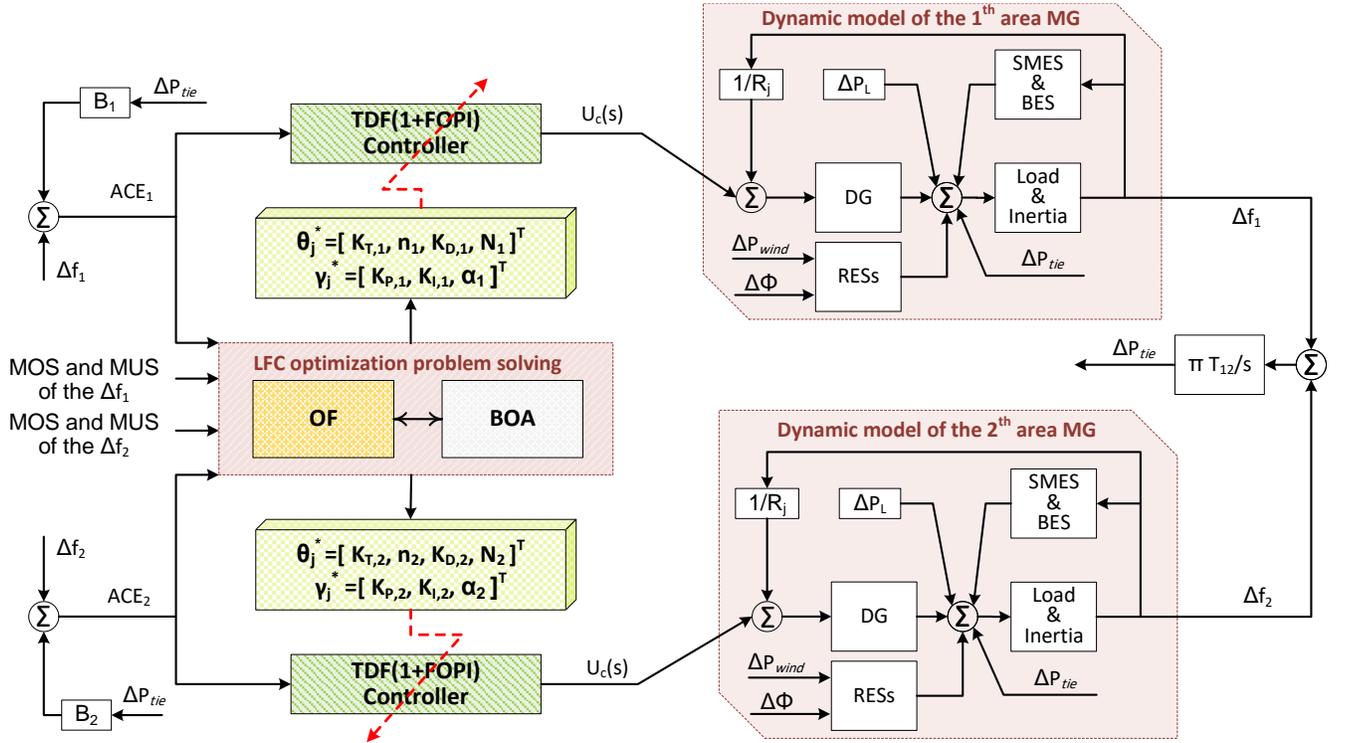
Fig. 4: Problem-solving process overview

Table. 2: Optimized controller parameters

Controller	Area	Parameters							
		K_T	n	K_D	N	K_P	K_I	α	K_{PP}
TDF(1+FOPI)	Area1	2.1521	1.78026	0.3415	357.4932	1.1618	2.7810	0.5095	
	Area2	2.2300	1.9294	0.4202	462.9319	1.3712	3.0141	0.5482	
PID	Area1	-	-	1.3067	90.7476	1.4186	3.5457	-	-
	Area2	-	-	1.7246	368.8572	2.3212	4.0010	-	-
TID	Area1	3.4989	3.6809	0.6596	284.0214	-	3.7679	-	-
	Area2	3.6900	4.0023	0.6894	200.5588	-	3.7800	-	-
PD(1+PI)	Area1	-	-	0.8297	369	2.9572	3.9650	-	0.6420
	Area2	-	-	0.8803	489	3.2710	4.1020	-	0.8743

Δf_1 signal, 60% for Δf_2 signal and 2.5% for ΔP_{tie} signal by the proposed control strategy, compared to the PID, TID and PD(1+PI) controllers.

(v) Mixed disturbances, uncertainties, and nonlinearity condition

So far, the consequences of various disruptions and uncertainties in four scenarios have been explored individually. In this scenario, we investigate a condition in which a chain of disturbances results in complicated control conditions. With a 12 ms delay ($\tau = 12\ ms$) in delivering/sending control signal, the M parameter is lowered by 35% in both areas while the D parameter is raised by 35% from nominal value. Disturbances in loans an RESs output power are assumed as shown in Fig. 13. The dynamic response of the system is illustrated in Fig. 14. Also, important time-domain indicators for numerical comparison are tabulated in Table 3. According to Table 3, the OF value where the proposed TDF(1+FOPI) controller is applied is about 64, 44, and 52% better than a situation that the PID, TID, and PD(1+PI) controllers are employed, respectively. On average, the ITSE indicator by TDF(1+FOPI) controller usage is diminished about 72%. This reduction for IAE indicator is about 53%.

(vi) Comparing with GOA optimized PID controller

In this scenario, to better compare the proposed control strategy, the performance of the TDF(1+FOPI) controller with the optimal PID controller introduced in [19] are compared. The system under study is similar to that introduced in Section 2, except that it has no SMES unit in either area. Sudden changes in the demand side in areas 1 and 2 have been applied in the magnitude of +0.2 and +0.7, respectively. Also, a time delay of 10 ms in receiving/sending the control signal is included. The controllers' optimal parameters are reported in Table 5. Also, Fig. 16 shows the dynamic response of the system with two controllers. The important evaluation indicators related to the dynamic response of the system are presented in Table 6 to compare the results more accurately. According to Table 6, it can be seen that although the damping speed of the perturbation created in area 2 is almost the same with both controllers, the ST for the frequency fluctuation signal of are 1 Δf_1 has been improved by more than 30%. Also, the maximum frequency deviation in areas 1 and 2 has been reduced by more than 25 and 15% using TDF(1+FOPI) controller, respectively.

6. CONCLUSION

The TDF(1+FOPI), a novel multistage controller based on FO control operators, is introduced in this paper. BOA is utilized to
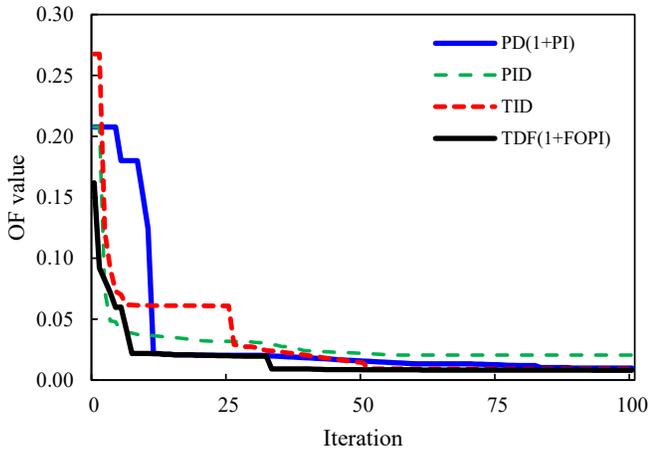
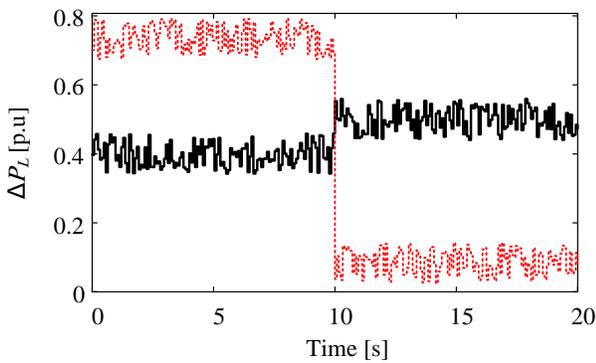Fig. 5: Convergence curve of the BOA for various controllers

Fig. 6: Power demand fluctuations. Solid: area1 and dashed: area2

(a)

(b)

(c)

Fig. 7: Power demand fluctuations. Solid: area1 and dashed: area2

optimize the controller's functionality when performing the LFC task. The employed cost function combines the ACE signal and the Δf_j dynamic characteristics, including MOS and MUS. The performance of the suggested control method is analyzed in six distinct working conditions. The TDF(1+FOPI) controller's quality is validated by comparing its performance to that of the PID, a controller with a tilting operator (TID), and a multistage controller (PD(1+PI)). When comparing the six scenarios in which the proposed LFC strategy is employed with other controlling methods, it is found that the OF value fell by an average of 56%. The average values of the ITSE and IAE indices, where the TDF(1+FOPI) controller is applied, are also 71 and 51% lower in these six cases, respectively. The proposed multistage FO controller improves the system's dynamic response characteristics, such as ST, OS, and US. It is shown in scenario (iv) that the Δf_1, Δf_2, and ΔP_{tie} signals' US decreased by an average of 48%, 56%, and 20% compared to the three other controllers, respectively.

The proposed controller has only two more handles than the multistage PD(1+PI) controller and three more handles than a conventional controller such as PID. However, the results show the dominance of the proposed control system over the PID, TID and PD(1+PI) controllers. The proposed TDF(1+FOPI) is a revolutionary controller with a simple structure that outperforms existing controllers by integrating common control operators in a multistage framework. It is a desirable choice for usage in complicated control processes like LFC tasks.

REFERENCES

[1] H. Shayeghi and A. Younesi, "Mini/Micro-Grid Adaptive Voltage and Frequency Stability Enhancement," *J. Oper. Auto. Power Eng.*, vol. 7, no. 1, pp. 107-118, 2019.
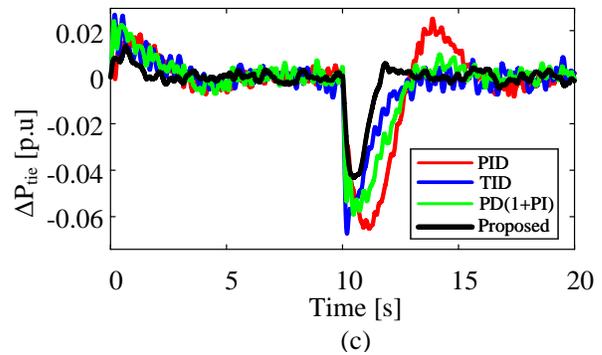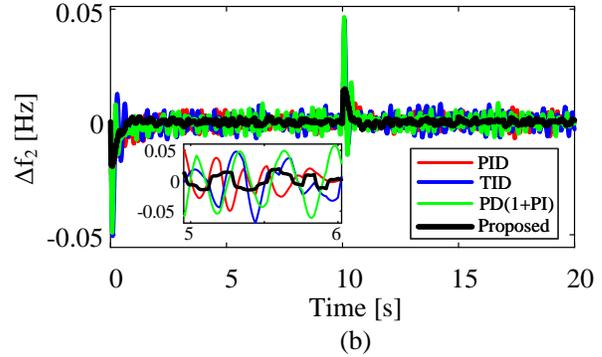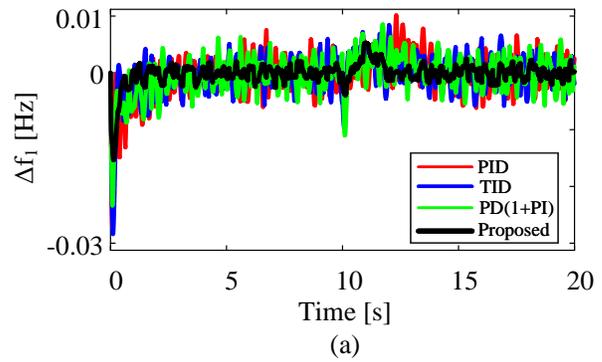
[2] H. Ali et al., "A new frequency control strategy in an islanded microgrid using virtual inertia control-based coefficient diagram method," *IEEE Access*, vol. 7, pp. 16979-16990, 2019.

[3] M. Ramesh, A. K. Yadav, and P. K. Pathak, "An extensive review on load frequency control of solar-wind based hybrid renewable energy systems," *Energy Sources Part A*, pp. 1-25, 2021.

[4] B. Long, Y. Liao, K. T. Chong, J. Rodríguez, and J. M. Guerrero, "MPC-controlled virtual synchronous generator to enhance frequency and voltage dynamic performance in islanded microgrids," *IEEE Trans. Smart Grid*, vol. 12, no. 2, pp. 953-964, 2020.

[5] M. Gheisarnejad and M. H. Khooban, "Secondary load frequency control for multi-microgrids: HiL real-time simulation," *Soft Computing*, vol. 23, no. 14, pp. 5785-5798, 2019.

[6] H. Bevrani, F. Habibi, P. Babahajyani, M. Watanabe, and Y. Mitani, "Intelligent Frequency Control in an AC Microgrid: Online PSO-Based Fuzzy Tuning Approach," *IEEE Trans. Smart Grid*, vol. 3, no. 4, pp. 1935-1944, 2012.

[7] H. Shayeghi and A. Younesi, "Fuzzy PID Control of Microgrids," *in Microgrid Archi., Control Prote. Methods. Cham: Springer Int. Publishing*, 2020, pp. 555-575.

[8] R. K. Khadanga, S. Padhy, S. Panda, and A. Kumar, "Design

Table. 3: Comparison of indicators value using various controllers

Case	Index	Controller			
		PID	TID	PD(1+PI)	TDF(1+FOPI)
(i)	OF	2.6162	2.0827	2.1936	1.1302
	ITSE×100	7.2824	4.3050	5.2786	1.7782
	IAE×10	2.9991	2.5680	2.6511	1.3675
	Max(|Δf_1|)	0.0220	0.2970	0.0274	0.0142
	Max(|Δf_2|)	0.0371	0.0555	0.0483	0.0195
(ii)	OF	3.1914	2.5660	2.5780	1.2342
	ITSE×100	3.8251	2.0673	2.4656	0.5976
	IAE×10	2.9688	2.2532	2.3277	1.1669
	Max(|Δf_1|)	0.0056	0.0052	0.0052	0.0035
	Max(|Δf_2|)	0.0038	0.0052	0.0042	0.0026
(iii)	OF	1.1958	0.8013	0.9044	0.4124
	ITSE×100	1.5888	0.5647	0.8641	0.2051
	IAE×10	2.0321	1.3708	1.5573	0.7420
	Max(|Δf_1|)	0.0045	0.0057	0.0051	0.0033
	Max(|Δf_2|)	0.0042	0.0061	0.0054	0.0027
(iv)	OF	0.2035	0.0727	0.0841	0.0324
	ITSE×100	0.2877	0.0516	0.0809	0.0309
	IAE×10	1.2828	0.6559	0.7744	0.4478
	Max(|Δf_1|)	0.0528	0.0556	0.0550	0.0281
	Max(|Δf_2|)	0.0405	0.0491	0.0483	0.0197
(v)	OF	3.2255	2.0328	2.3772	1.1337
	ITSE×100	8.1042	3.5729	4.4110	1.3119
	IAE×10	3.5623	2.3965	2.7059	1.3189
	Max(|Δf_1|)	0.0095	0.0067	0.0073	0.0052
	Max(|Δf_2|)	0.0111	0.0101	0.0106	0.0035
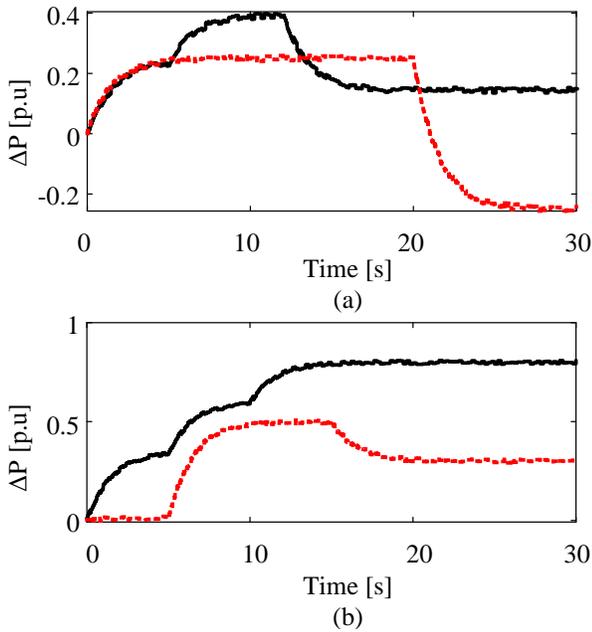
Fig. 8: RESs output power in scenario (ii). (a) PV and (b) WT. Solid: area1, dashed: area2

Fig. 9: Dynamic response of the system in scenario (ii)

Table. 4: Dynamic response characteristics in scenario (iv)

Signal	Index	Controller			
		PID	TID	PD(1+PI)	Proposed
Δf_1	Settling time	2.9224	1.5716	2.1632	1.9590
	Undershoot	0.0528	0.0556	0.0550	0.0281
	Overshoot	0.0081	0.0014	0.0075	0.0021
Δf_2	Settling time	2.7399	2.7865	3.0476	1.1285
	Undershoot	0.0405	0.0491	0.0483	0.0197
	Overshoot	0.0092	0.0035	0.0107	0.0001
ΔP_{tie}	Settling time	7.5497	2.8658	6.0660	4.5147
	Undershoot	0.0381	0.0263	0.0270	0.0235
	Overshoot	0.0101	0.0002	0.0019	0.0031

and analysis of tilt integral derivative controller for frequency control in an islanded microgrid: a novel hybrid dragonfly and pattern search algorithm approach," *Arab. J. Scie. Eng.*, vol. 43, no. 6, pp. 3103-3114, 2018.

[9] A. Latif, S. M. S. Hussain, D. C. Das, T. S. Ustun, and A. Iqbal, "A review on fractional order (FO) controllers optimization for load frequency stabilization in power networks," *Energy Reports*, vol. 7, pp. 4009-4021, 2021.

[10] A. Singh and S. Suhag, "Frequency regulation in an AC microgrid interconnected with thermal system employing multiverse-optimised fractional order-PID controller," *Int. J. Sustainable Energy* , vol. 39, no. 3, pp. 250-262, 2020.
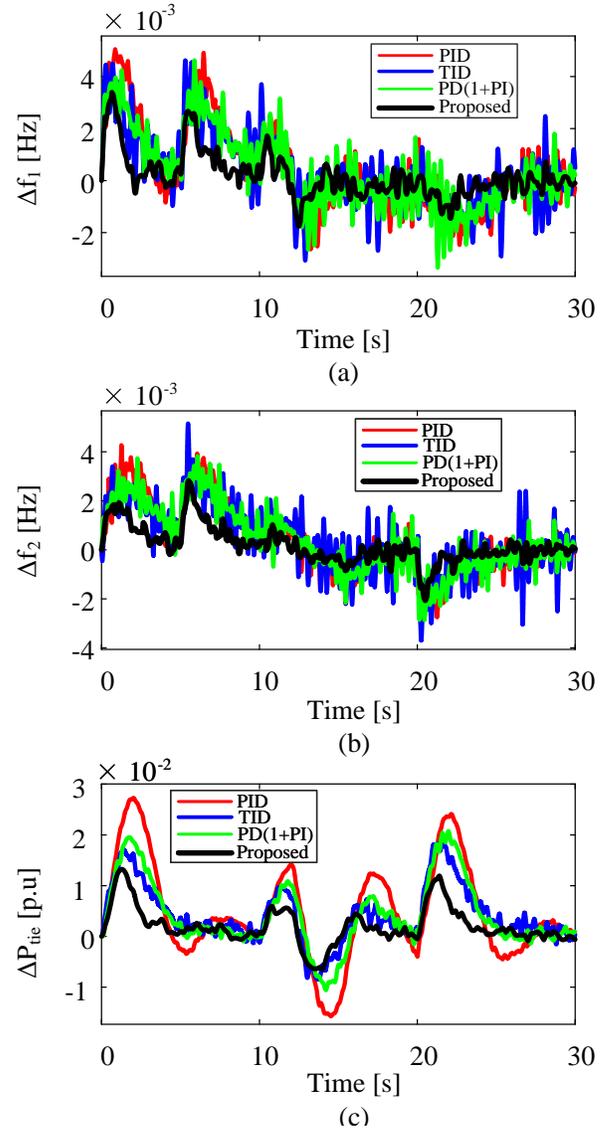
[11] A. izadbakhsh, s. khorashadizadeh, and P. Kheirkhahan, "Real-time Fuzzy Fractional-Order Control of Electrically Driven Flexible-Joint Robots," *AUT J. Modeling Simul.*, vol. 52, no. 1, pp. 2-2, 2020.

[12] A. Koszewnik, E. Pawłuszewicz, and M. Ostaszewski, "Experimental studies of the fractional PID and TID controllers

Table. 5: Optimal controller parameters in case (vi)

Controller	Area	Parameters						
		K_T	n	K_D	N	K_P	K_I	α
TDF(1+FOPI)	Area1	1.5012	2.0745	0.2820	349.3467	0.6770	1.4147	0.6009
	Area2	1.2657	2.6275	0.2840	464.9677	1.4461	2.1212	0.6891
PID	Area1	-	-	0.5019	-	0.3823	9.9998	-
	Area2	-	-	0.4159	-	0.3149	9.9274	-
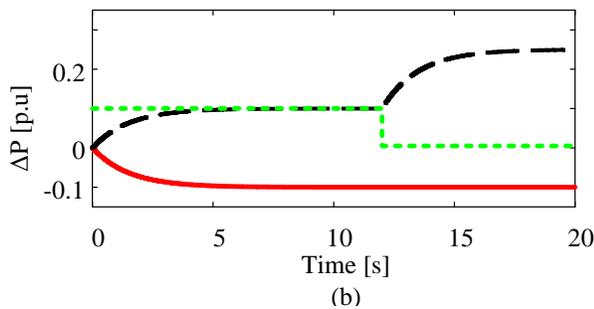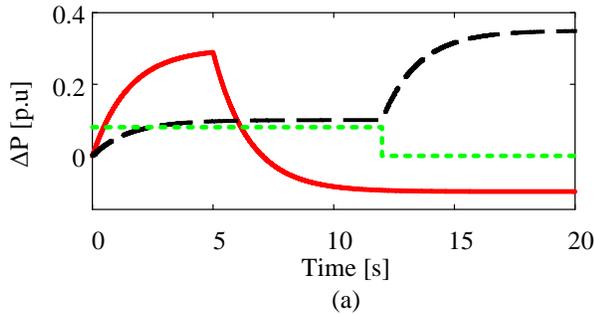
Fig. 10: Applied disturbances in scenario (iii). (a) area1 and (b) are2. Solid: ΔP_{PV}, dashed: ΔP_{WT}, and dotted: ΔP_L

Table. 6: Evaluation indexes of the system dynamic response in case (vi)

Index	Controller	
	PID	TDF(1+FOPI)
OF	0.2615	0.2038
ITSE×100	1.0621	0.7921
IAE×10	2.3680	1.8401
Max(|Δf_1|)	0.1026	0.0746
Max(|Δf_2|)	0.0210	0.0175
ST(Δf_1)	3.5404	2.3550
ST(Δf_2)	3.5243	3.5047

Fig. 11: Dynamic response of the system in scenario (iii)

for industrial process," *I. J. Control, Auto. Syst.*, vol. 19, no. 5, pp. 1847-1862, 2021.

[13] F. Babaei and A. Safari, "SCA based Fractional-order PID Controller Considering Delayed EV Aggregators," *J. Oper. Auto. Power Eng.*, vol. 8, no. 1, pp. 75-85, 2020.

[14] R. K. Khadanga, S. Padhy, S. Panda, and A. Kumar, "Design and analysis of multi-stage PID controller for frequency control in an islanded micro-grid using a novel hybrid whale optimization-pattern search algorithm," *Int. J. Nume. Model.: Electron. Net. Devices Fields*, vol. 31, no. 5, p. e2349, 2018.

[15] H. Shayeghi and A. Rahnama, "Designing a PD-(1+PI) Controller for LFC of an Entirely Renewable Microgrid Using PSO-TVAC," *Int. J. "Techni. Physi. Prob. Eng." (IJTPE)*, vol. 12, no. 45, pp. 19-27, 2020.

[16] B. Khokhar, S. Dahiya, and K. Singh Parmar, "A robust Cascade controller for load frequency control of a standalone microgrid incorporating electric vehicles," *Elec. Power Compo.*
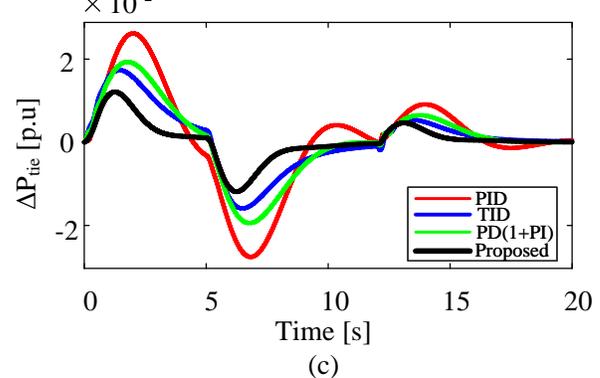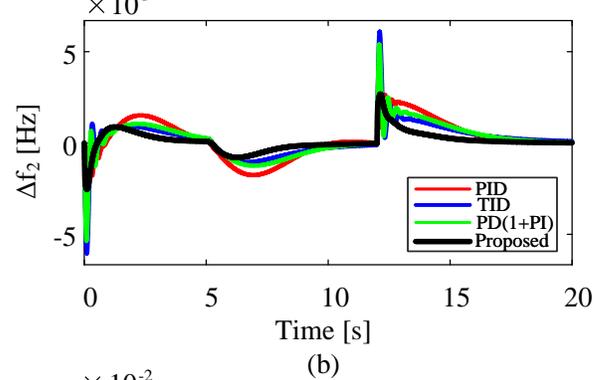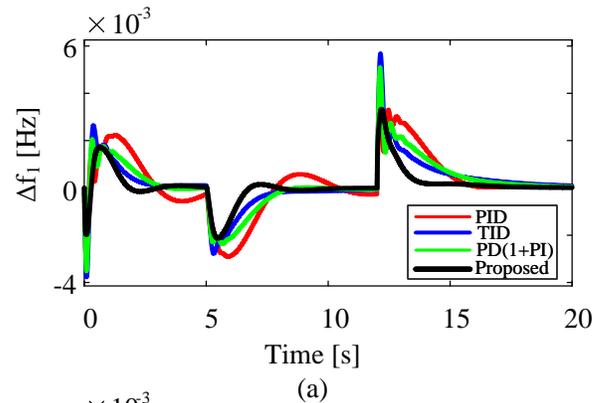
Syst., vol. 48, no. 6-7, pp. 711-726, 2020.

[17] Zaheeruddin and K. Singh, "Intelligent fractional-order-based centralized frequency controller for microgrid," *IETE J. Res.*, pp. 1-15, 2020.

[18] H. Shayeghi, A. Rahnama, and H. H. Alhelou, "Frequency control of fully-renewable interconnected microgrid using fuzzy cascade controller with demand response program considering," *Energy Reports*, vol. 7, pp. 6077-6094, 2021.

[19] D. K. Lal, A. K. Barisal, and M. Tripathy, "Load Frequency Control of Multi Area Interconnected Microgrid Power System
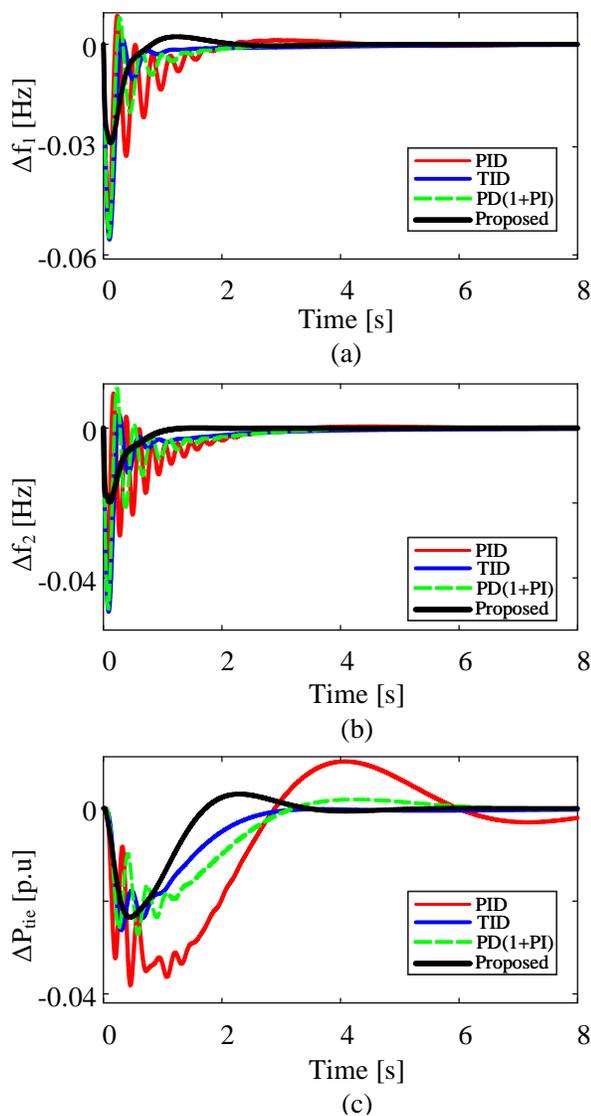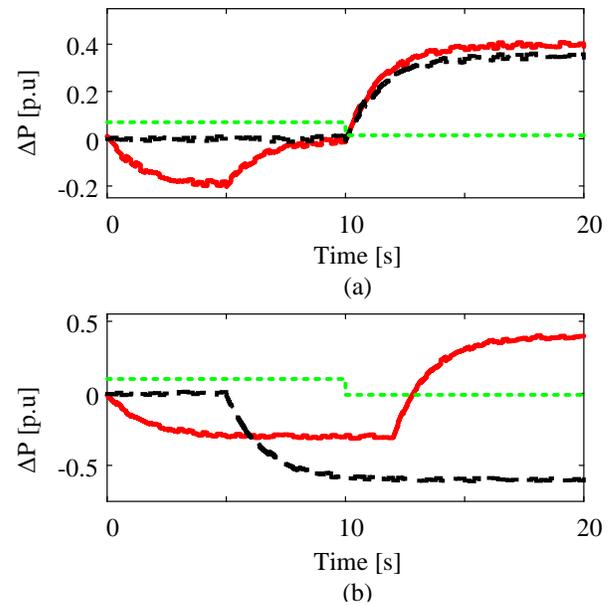
Fig. 12: Dynamic response of the system in scenario (iv)

Fig. 13: Applied disturbances in scenario (v) (a) area1 and (b) are2. Solid: ΔP_{PV}, dashed: ΔP_{WT}, and dotted: ΔP_L

using Grasshopper Optimization Algorithm Optimized Fuzzy PID Controller," *in 2018 Recent Adv. Eng., Techno. Computa. Sci. (RAETCS)*, 6-8 Feb. 2018 2018, pp. 1-6.

[20] A. Younesi and H. Shayeghi, "Q-Learning Based Supervisory PID Controller for Damping Frequency Oscillations in a Hybrid Mini/Micro-Grid," *Iran. J. Elec. Electron. Eng.*, vol. 15, no. 1, pp. 126-141, 2019, doi: 10.22068/IJEEE.15.1.126.

[21] S. Roozbehani, M. T. Hagh, and S. G. Zadeh, "Frequency control of islanded wind-powered microgrid based on coordinated robust dynamic droop power sharing," *IET Gener. Transmi. Dist.*, vol. 13, no. 21, pp. 4968-4977, 2019.

[22] H. Abubakr, T. H. Mohamed, M. M. Hussein, J. M. Guerrero, and G. Agundis-Tinajero, "Adaptive frequency regulation strategy in multi-area microgrids including renewable energy and electric vehicles supported by virtual inertia," *Int. J. Elec. Power & Energy Syst.*, vol. 129, p. 106814, 2021.

[23] H. Ali, G. Magdy, and D. Xu, "A new optimal robust controller for frequency stability of interconnected hybrid microgrids considering non-inertia sources and uncertainties," *Int. J. Elec. Power & Energy Syst.*, vol. 128, p. 106651, 2021.

[24] A. D. Shakibjoo, M. Moradzadeh, and S. Z. Moussavi, "A Novel Technique for Load Frequency Control of Multi-Area

Power Systems," *Energies*, vol. 13, no. 9, 2020.

[25] S. Mishra, R. C. Prusty, and S. Panda, "Design and Analysis of 2dof-PID Controller for Frequency Regulation of Multi-Microgrid Using Hybrid Dragonfly and Pattern Search Algorithm," *J. Control, Auto. Elec. Syst.*, vol. 31, no. 3, pp. 813-827, 2020.

[26] S. Padhy and S. Panda, "Application of a simplified Grey Wolf optimization technique for adaptive fuzzy PID controller design for frequency regulation of a distributed power generation system," *Prote. Control Modern Power Syst.*, vol. 6, no. 1, pp. 1-16, 2021.

[27] M. A. Sobhy, A. Y. Abdelaziz, H. M. Hasanien, and M. Ezzat, "Marine predators algorithm for load frequency control of modern interconnected power systems including renewable energy sources and energy storage units," *Ain Shams Eng. J.* , vol. 12, no. 4, pp. 3843-3857, 2021.

[28] P. C. Nayak, U. C. Prusty, R. C. Prusty, and A. K. Barisal, "Application of SOS in fuzzy based PID controller for AGC of multi-area power system," *in 2018 Techn. Smart-City Energy Secu. Power (ICSESP)*, 2018, pp. 1-6.

[29] S. Kayalvizhi and D. M. V. Kumar, "Load Frequency Control of an Isolated Micro Grid Using Fuzzy Adaptive Model Predictive Control," *IEEE Access*, vol. 5, pp. 16241-16251, 2017

[30] A. K. Das and D. K. Pratihar, "Bonobo optimizer (BO): an intelligent heuristic with self-adjusting parameters over continuous spaces and its applications to engineering problems," *Applied Intel.*, vol. 52, no. 3, pp. 2942-2974, 2022.

[31] R. Dadi, K. Meenakshy, and S. Damodaran, "A Review on Secondary Control Methods in DC Microgrid," *J. Oper. Autom. Power Eng.*, 2022.

[32] M. Khooban, "Secondary Load Frequency Control of Time-Delay Stand-Alone Microgrids With Electric Vehicles," *IEEE Trans. Ind. Electron.* , vol. 65, no. 9, pp. 7416-7422, 2018, doi: 10.1109/TIE.2017.2784385.

[33] T. Gönen, "Distributed Generation and Renewable Energy," *in Elec. Power Dist. Eng., Third ed.: CRC Press, Tylor & Francis Group*, 2014, pp. 767-834.

[34] D. C. Das, A. Roy, and N. Sinha, "GA based frequency controller for solar thermal–diesel–wind hybrid energy generation/energy storage system," *Int. J. Elec. Power &*
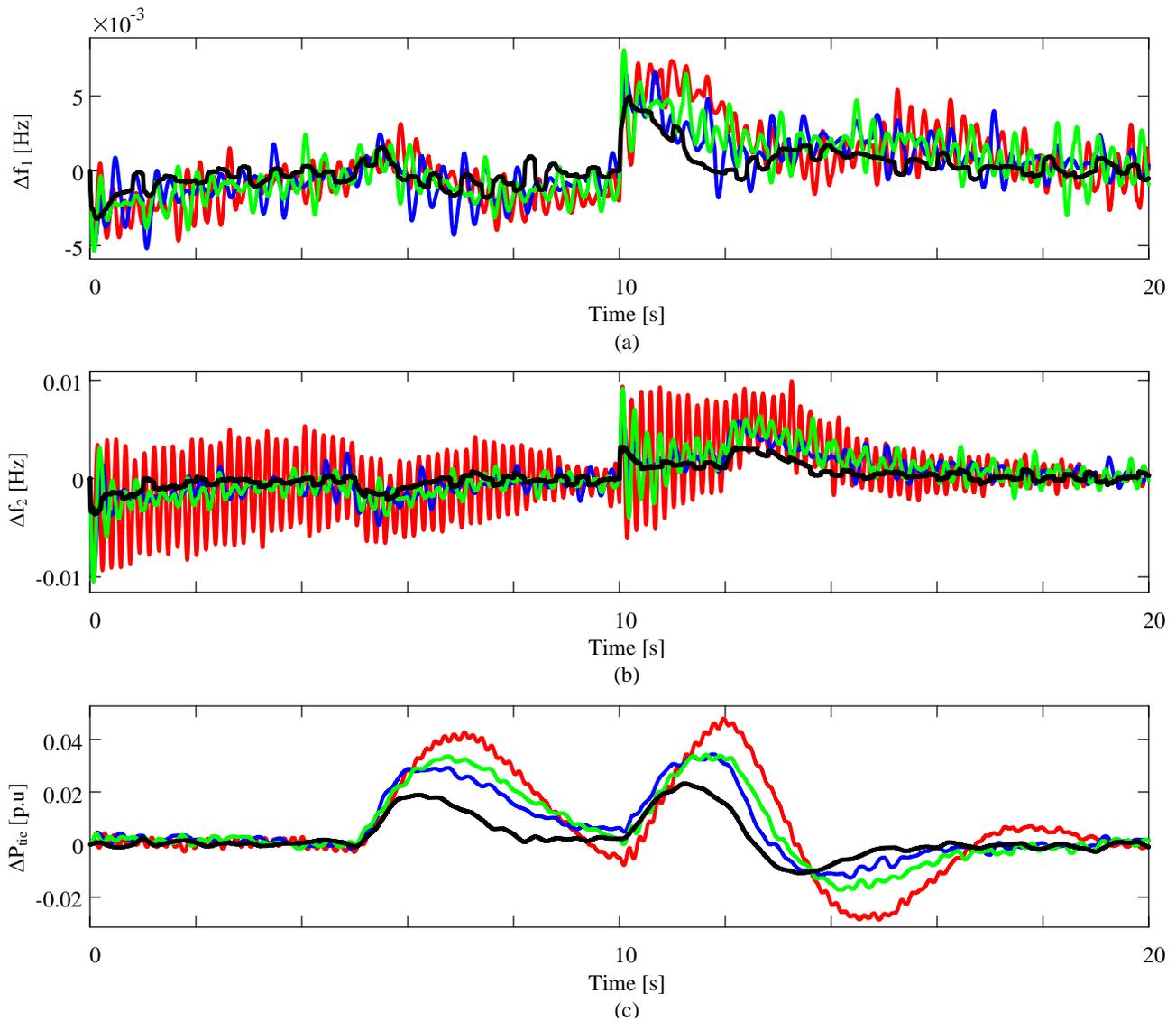
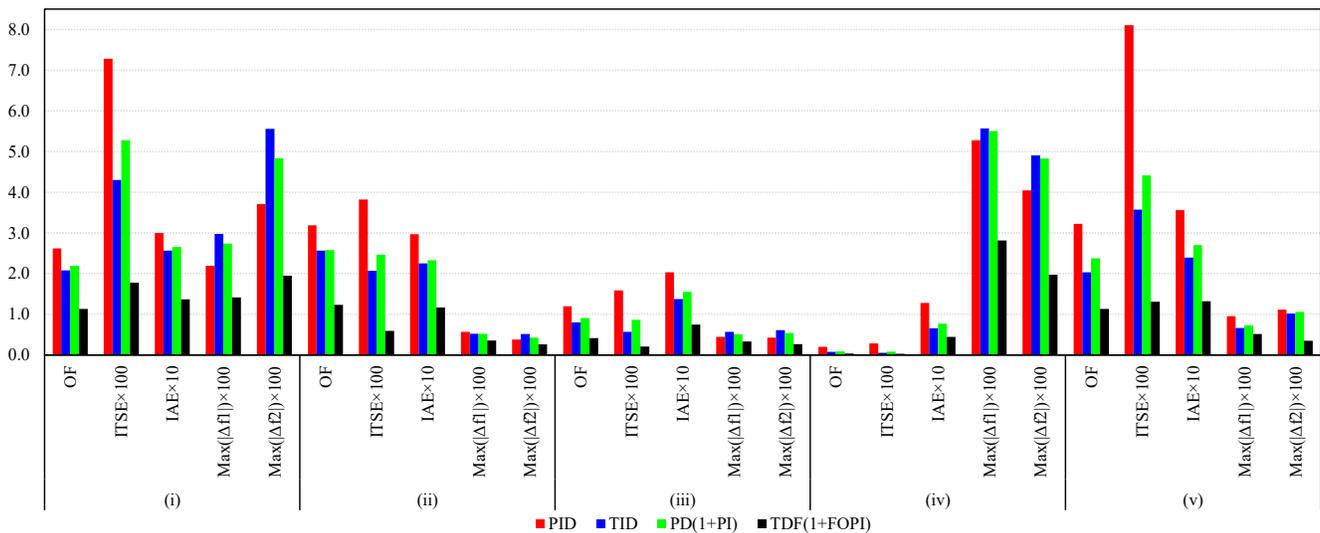Fig. 14: Dynamic response of the system in scenario (v)
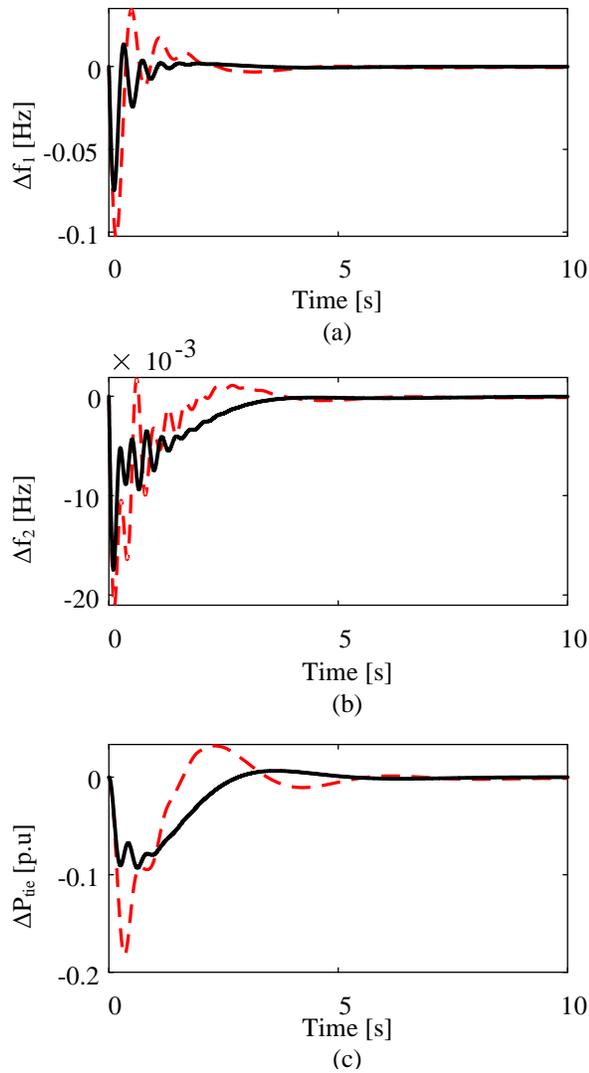

Fig. 15: Indicator's value in five scenarios

Fig. 16: Dynamic response of the system in scenario (vi)

Energy Syst., vol. 43, no. 1, pp. 262-279, 2012.

[35] A. Demirören, "Application of a self-tuning to automatic generation control in power system including smes units," *Eur. Trans. Electr. Power* , vol. 12, no. 2, pp. 101-109, 2002

[36] C. A. Monje, Y. Chen, B. M. Vinagre, D. Xue, and V. Feliu-Batlle, Fractional-order systems and controls: fundamentals and applications. *Springer Sci. Busin. Media*, 2010.

[37] P. N. Topno and S. Chanana, "Differential evolution algorithm based tilt integral derivative control for LFC problem of an interconnected hydro-thermal power system," *J. Vib. Control* , vol. 24, no. 17, pp. 3952-3973, 2018.

[38] P. Warrier and P. Shah, "Fractional order control of power electronic converters in industrial drives and renewable energy systems: a review," *IEEE Access*, 2021.

[39] A. Tepljakov, "FOMCON: fractional-order modeling and control toolbox," *Fract. ord. modeling control dyna. syst.: Springer*, 2017, pp. 107-129.